International Journal of Microwave and Wireless Technologies

cambridge.org/mrf

Analysis of transmission performance on wireless power transfer system with metamaterial

Xingming Fan, Haonan Zhang and Xin Zhang

Department of Electrical Engineering and Automation, Guilin University of Electronic Technology, Guilin, China

Research Paper

Cite this article: Fan X, Zhang H, Zhang X (2024) Analysis of transmission performance on wireless power transfer system with metamaterial. *International Journal of Microwave and Wireless Technologies* **16**(1), 83–91. https://doi.org/10.1017/S1759078723000582

Received: 19 December 2022
Revised: 15 April 2023
Accepted: 20 April 2023

Keywords:
magnetic coupling resonant wireless power transfer; metamaterial; multilayer; power transfer efficiency

Corresponding author:
Xin Zhang,
Email: plxxaim@guet.edu.cn

Abstract

In order to solve the problems of low power transfer efficiency (PTE) and limited distance in magnetic coupling resonant wireless power transfer (MCR-WPT) technology. In this paper, based on the magnetic field control ability of metamaterials (MMs), the way to improve the performance of MCR-WPT systems is studied. First, the influence of MMs on the coupling of MCR-WPT system is theoretically analyzed by establishing an equivalent circuit model. Through a series of simulations and experiments, the relationships between the PTE and the array and placement of the MM slab are investigated. The results demonstrate that when one MM slab is placed in the middle, near the Tx coil or the Rx coil, the optimal PTE can be obtained by inserting one slab with 6×6, 1×1, and 6×6 arrays, respectively. Moreover, the systems with multilayer MM slabs are also studied. The measured PTEs on one, two, and three layers of MM slabs can increase by 20.6%, 29.3%, and 22.6%, respectively. The efficiency improvement capability of one MM slab is better than three slabs but worse than two slabs. This paper discusses the application of MMs in MCR-WPT systems, which has a certain reference significance.

Introduction

Wireless power transfer (WPT) is a novel energy transfer technology that transfers electrical energy from the power source to a load without direct contact with charging equipment. WPT technology avoids the deficiencies of traditional wired power transfer, such as poor flexibility and low safety. In 2007, Soljacic's proposed a magnetic coupling resonant WPT (MCR-WPT) technology [1]. This technology is based on magnetic resonance theory and relies on near-field resonant coupling. Because MCR-WPT technology has the advantages of moderate transmission distance and power, it has been employed in electric vehicles, medical equipment, and portable electronic products [2–4]. However, the power transfer efficiency (PTE) drops dramatically as the distance increases. Improving transmission performance has become a research topic for MCR-WPT technology.

Currently, there are several approaches to improve the PTE of MCR-WPT systems, including designing a high-Q resonant coil and adding a relay coil or metamaterial (MM) slab [5–7]. As a composite material, MMs have many exotic properties, including the Doppler effect, inverse Cherenkov radiation, and negative refraction index [8]. Therefore, it has been used in a wide range of fields including invisible cloak, superlens, and magnetic resonance imaging [9–11]. The negative refraction index has shown great potential in the MCR-WPT technology because it can enhance evanescent waves and improve the coupling between coils. In 2010, Choi *et al.* proposed an MM with a real part of permeability equal to −1 [12]. It was demonstrated that the negative permeability MM was used to improve the PTE of MCR-WPT systems. Urzhumov presented a theoretical analysis on the MCR-WPT system with MM, in which the coil was regarded as a magnetic dipole and the MM slab as infinite [13]. It indicates that even if MMs have a loss, the PTE of systems with the MM will be higher than that of the original system. In addition, the effect of different MM structures on the PTE of systems was investigated by Li et al. [14], and the results showed that the ranking of the four structures on performance improvement of the system is as follows: 3D > 2-slab > 1-slab > 2D. Although a great deal of work has been carried out on the MCR-WPT system with MMs, there are few studies on the influence of the period, position, and layer of MM slabs on the system.

In this work, the influence of the MM on PTE of the MCR-WPT system is investigated to improve its performance. First, the regulation principle of the MM in the electromagnetic field is theoretically analyzed. The MCR-WPT system working at 6.78 MHz is built in the high-frequency simulation software HFSS. A negative permeability MM with the advantages of lightweight and small size is designed and fabricated to meet the requirements of the system. Then, six arrays of slabs are constructed by MM units, which are placed in different positions of the system to evaluate the impact of MMs on PTEs under different conditions. The experimental measurements show that the highest PTE improvement increases by 20.6% through inserting

© The Author(s), 2023. Published by Cambridge University Press in association with the European Microwave Association

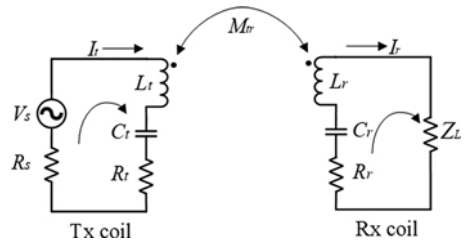


Figure 1. The equivalent circuit diagram of dual-coil MCR-WPT system.

a 6×6 MM slab in the middle. When the MM slab is near the Tx coil or Rx coil, a 1 × 1 or 6 × 6 MM slab should be used for the optimal PTE, respectively. Beyond that, the systems with two MM slabs and three MM slabs are also investigated. The measured PTEs of the systems with two slabs and three slabs increase by 29.3% and 22.6%, respectively. The experiment results show that the improvement of two MM slabs is better than one slab and three slabs.

Analysis of MCR-WPT system with MM

Theoretical analysis on a dual-coil MCR-WPT system with MM

Circuit theory and coupled mode theory are general methods to evaluate the transmission performance of MCR-WPT systems. Compared with the four-coil MCR-WPT system, the dual-coil system has the advantages of simple structure and excellent space occupation, so the dual-coil MCR-WPT system is analyzed, which consists of Tx and Rx coils. According to the equivalent circuit theory, the plane spiral coil can be regarded as a circuit composed of resistance, capacitance, and inductance, and the equivalent circuit diagram is shown in Fig. 1.

M_{tr} is the mutual inductance between Tx and Rx coils. $V_{\mathrm{s}}, R_{\mathrm{s}}$, and Z_{L} represent power source and source resistance and load resistance, respectively. $R_{\mathrm{t}}, L_{\mathrm{t}}$, and C_{t} denote the resistance, inductance, and capacitance of the Tx coil, respectively. $R_{\mathrm{r}}, L_{\mathrm{r}}$, and C_{r} denote the resistance, inductance, and capacitance of the Rx coil, respectively. According to the equivalent circuit model, the KVL equation can be obtained

$$\begin{cases} \left(R_{\mathrm{s}} + j\omega L_{\mathrm{t}} + R_{\mathrm{t}} + \frac{1}{j\omega C_{\mathrm{t}}}\right) I_{\mathrm{t}} - j\omega M_{\mathrm{tr}} I_{\mathrm{r}} = V_{\mathrm{s}} \\ \left(R_{\mathrm{r}} + j\omega L_{\mathrm{r}} + Z_{\mathrm{L}} + \frac{1}{j\omega C_{\mathrm{r}}}\right) I_{\mathrm{r}} - j\omega M_{\mathrm{tr}} I_{\mathrm{t}} = 0 \end{cases} \tag{1}$$

In a deep subwavelength, MMs can also be represented by *RLC* circuits. The capacitance is derived from the scattered field formed between the resonator, and the inductance is determined by the induced current distribution of the resonator structure. The resistance and induced current distribution are related to the ohmic loss of the unit. Thus, the equivalent circuit diagram of a dual-coil MCR-WPT system with MMs is represented in Fig. 2.

By using the equivalent circuit theory and the mutual coupling theory, the KVL equations of the MCR-WPT system with MMs can be shown as follows:

$$\begin{cases} \left(R_{\mathrm{s}} + j\omega L_{\mathrm{t}} + R_{\mathrm{t}} + \frac{1}{j\omega C_{\mathrm{t}}}\right) I_{\mathrm{t}} + j\omega M_{\mathrm{ti}} I_i + j\omega M_{\mathrm{tr}} I_{\mathrm{r}} = V_{\mathrm{s}} \\ j\omega M_{\mathrm{ti}} I_{\mathrm{t}} + \left(R_i + j\omega L_i + \frac{1}{j\omega C_i}\right) I_i + j\omega M_{ij} I_j + j\omega M_{ri} I_{\mathrm{r}} = 0 \\ \left(R_{\mathrm{r}} + j\omega L_{\mathrm{r}} + Z_{\mathrm{L}} + \frac{1}{j\omega C_{\mathrm{r}}}\right) I_{\mathrm{r}} + j\omega M_{ri} I_i - j\omega M_{\mathrm{tr}} I_{\mathrm{t}} = 0 \end{cases} \tag{2}$$

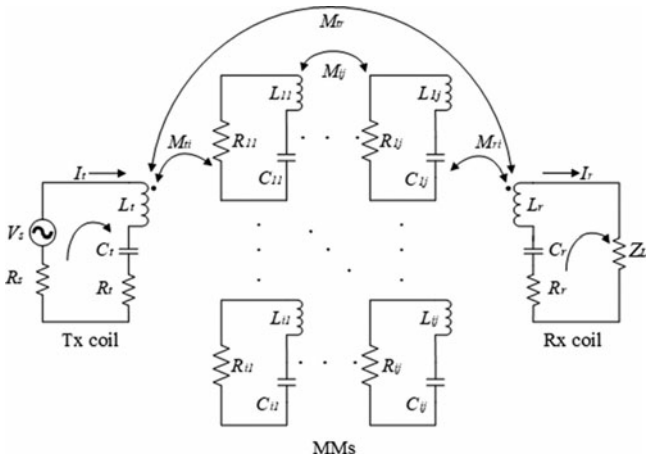


Figure 2. The equivalent circuit diagram of a dual-coil MCR-WPT system with MMs.

M_{ti} and M_{ri} represent the mutual inductance between the Tx coil and the ith unit and the mutual inductance between the Rx coil and the ith unit, respectively. M_{ij} is the mutual inductance between the ith unit and the jth unit ($i \neq j$).

Electromagnetic field regulation of MMs

It is known from Maxwell's equations that for conventional materials, their wave vector {**k**, electric vector {**E**, and magnetic field {**H** obey the right-handed rule. In 1967, Veselago predicted the properties of left-handed materials [15], that is, materials with negative permittivity and permeability. It was not until 2001 that Smith experimentally proved that left-handed material has a negative refractive index [16].

According to Snell's Law, reflection and refraction occur when electromagnetic waves are incident from one media to another. Assuming that both media are conventional materials, the incident wave and the refracted wave will lie on both sides of the normal. If a medium is a left-handed material, the refracted wave and the incident wave will be on the same side of the normal because of the need to meet the requirements of the continuity boundary condition, as shown in Fig. 3.

Considering the negative refraction effect of the MM, if it is placed between the Tx coil and Rx coil, the magnetic field induced by the current in the Tx coil passes through the MM and undergoes negative refraction to concentrate the magnetic field around the Rx coil. For the MCR-WPT system without the MM slab, the magnetic field will diverge during propagation, as shown in Fig. 4. When adding an MM slab in the system, the magnetic field distribution near the Rx coil is significantly improved. In other words, MMs increase the PTE of the MCR-WPT system by improving the magnetic field density and enhancing the coupling of the resonant coils.

Application of negative permeability MM in MCR-WPT system

Design of MCR-WPT system with MMs

Based on the practical application of wireless charging, a dual-coil MCR-WPT system with resonant frequency at 6.78 MHz is proposed, and their structural parameters as shown in Table 1. The Tx coil and Rx coil are both planar spiral coils wound with copper

https://doi.org/10.1017/S1759078723000582 Published online by Cambridge University Press

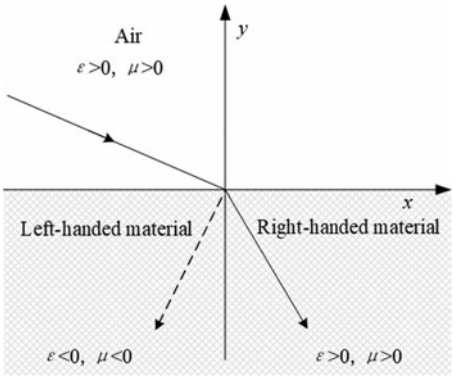


Figure 3. Schematic diagram of interface refraction.

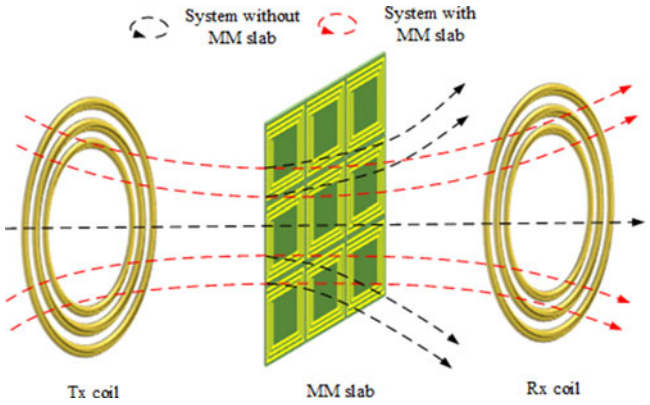


Figure 4. Magnetic field enhancement effect of resonant coils based on MM slab.

Table 1. Geometry parameters of Tx and Rx coils

Parameters	Value
Coil outer diameter	35 cm
Coil inner diameter	20 cm
Turn	8
Copper tube radius	3 mm
Turn spacing	8 mm
Resonant frequency	6.78 MHz

tubes, which have the advantages of compact structure and easy installation.

MMs have both negative permittivity and permeability; however, in a deep subwavelength, the magnetic field and electric field are decoupled. Therefore, the amplification of evanescent waves can be realized only by promising that the effective permeability is negative [17]. In general, MMs are composed of substrate and resonator. When electromagnetic waves are vertically incident on the surface of MMs, a circular current will be induced on the resonator and charges will also accumulate in the gaps of the spiral turns. At this point, the MM can be regarded as the *RLC* resonant circuit, which conforms to the like-Lorentz model to produce a negative permeability [18].

Since the constitutive parameters of the MM are determined by its structure, the permeability will change with its structural parameters. Figure 5 shows the relationship between the

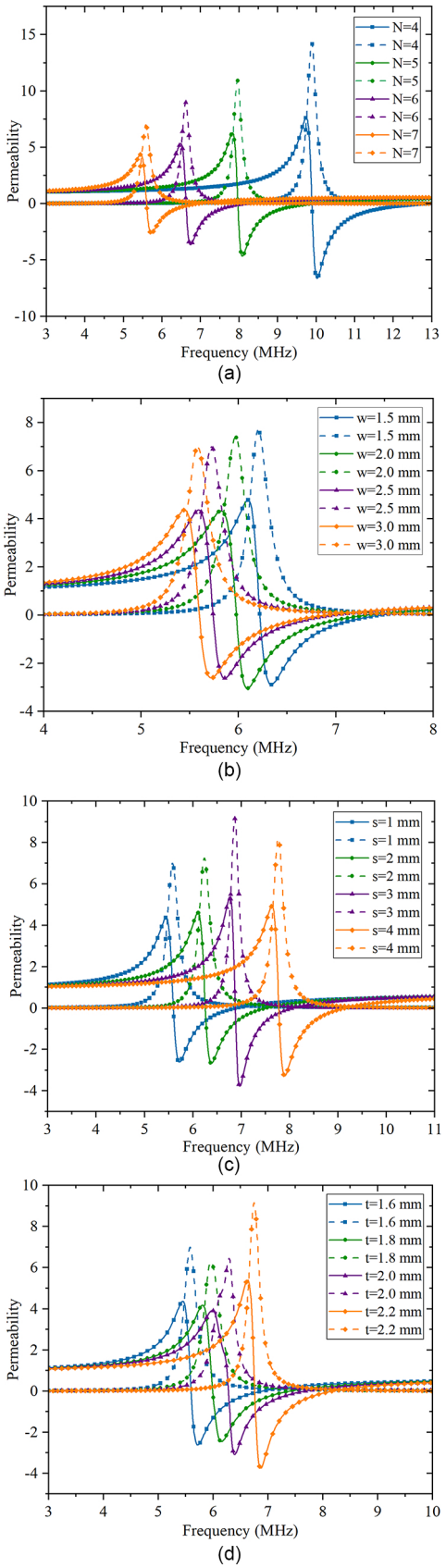


Figure 5. Effective permeability of the MM with different structure parameter variation: (a) turn of spiral *N*, (b) line width of spiral *w*, (c) line spacing of spiral *s*, and (d) thickness of substrate *t*.

https://doi.org/10.1017/S1759078723000582 Published online by Cambridge University Press

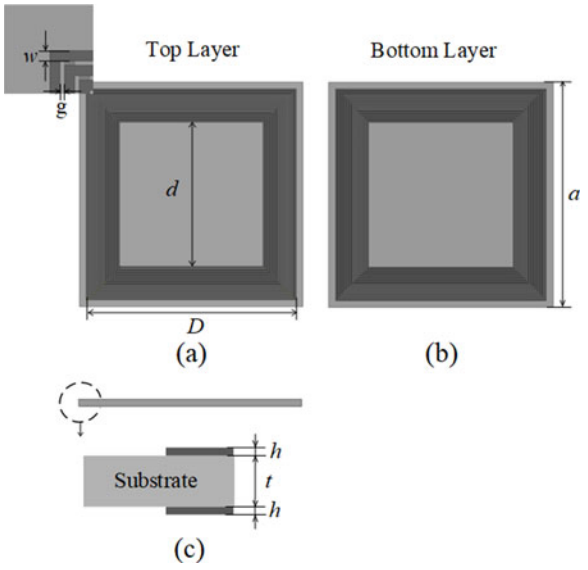


Figure 6. Geometry of the MM: (a) top view, (b) bottom view, and (c) side view.

permeability of the MM and its structural parameters; the solid line represents the real part of the effective permeability and the dashed line represents the imaginary part. It is worth noting that when one parameter is changed, the rest remains unchanged. When the number of spiral turns N increases, the capacitance and inductance of the MM also increase and the resonant frequency and permeability decrease. If the line width w of the spiral increases, the resonant frequency also decreases. Increasing the line spacing s will reduce the coupling between the spirals, contributing to the resonant frequency shift to high. In addition, the purpose of reducing the resonant frequency can also be achieved by decreasing the thickness t of the substrate.

Based on the above analysis, the design rules of MMs can be summarized that increasing the number of turns and line width of the spirals will reduce the resonant frequency; on the contrary, increasing the spacing of the spirals and the thickness of the substrate will increase the resonant frequency.

In order to satisfy the needs of the MCR-WPT system, an MM with a real part of effective permeability of −1 at 6.78 MHz is proposed according to the design rules, in which the substrate is an FR-4 and the resonators are copper. The resonators are etched on both sides of the substrate by the printed circuit board, and the structure is shown in Fig. 6. In this way, not only low-frequency MM can be obtained but also the coupling between the topological structures on both sides can be enhanced [19], and the specific structural parameters are shown in Table 2.

From the above analysis, it can be concluded that increasing the number of turns and line width of the spirals will reduce the resonant frequency; on the contrary, increasing the spacing of the spirals and the thickness of the substrate will increase the resonant frequency.

The negative permeability MM is optimized and designed in the high-frequency magnetic field simulation software HFSS by using full-wave simulations. Then the effective permeability is calculated by the S-parameter retrieval based on the Kramers–Kronig relationship [20, 21], and the real and imaginary parts of the permeability are extracted, respectively. Figure 7 shows the effective permeability of the MM; the real part is negative at 6 to 8.1 MHz, where the real and imaginary parts are −1 and 0.45i at 6.78 MHz, respectively. The imaginary part of the permeability represents its loss.

Table 2. Geometry parameters of Tx and Rx coils

Symbol	Parameters	Value
a	Length of side	65 mm
N	Turn	15
D	Outer spiral length	60 mm
d	Inner spiral length	42 mm
w	Line with	0.5 mm
g	Line spacing	0.3 mm
h	Copper thickness	0.035 mm
t	Substrate thickness	1.6 mm

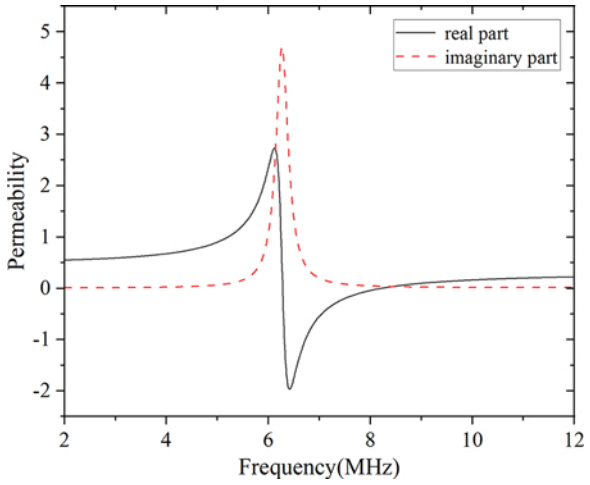


Figure 7. Effective permeability of the MM.

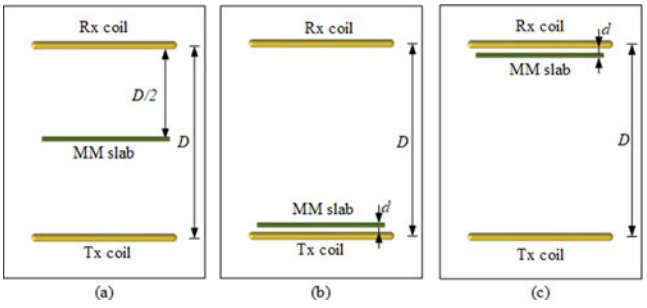


Figure 8. Schematic diagram of MM slab placed at different positions of the MCR-WPT system: (a) in the middle, (b) near the Tx coil, and (c) near the Rx coil.

Simulations of MCR-WPT system with MMs

In order to study the influence of MMs on the PTE of the MCR-WPT system, the focusing effect of MM slab with various arrays on the PTE of the system when they are inserted in different positions are studied; the three positions are shown in Fig. 8. The MM-based MCR-WPT system consists of the Tx coil, the Rx coil, and MM slabs, where D is the transmission distance between Tx and Rx coils and d is the distance from the MM slab to the coil, fixed at 5 cm.

https://doi.org/10.1017/S1759078723000582 Published online by Cambridge University Press

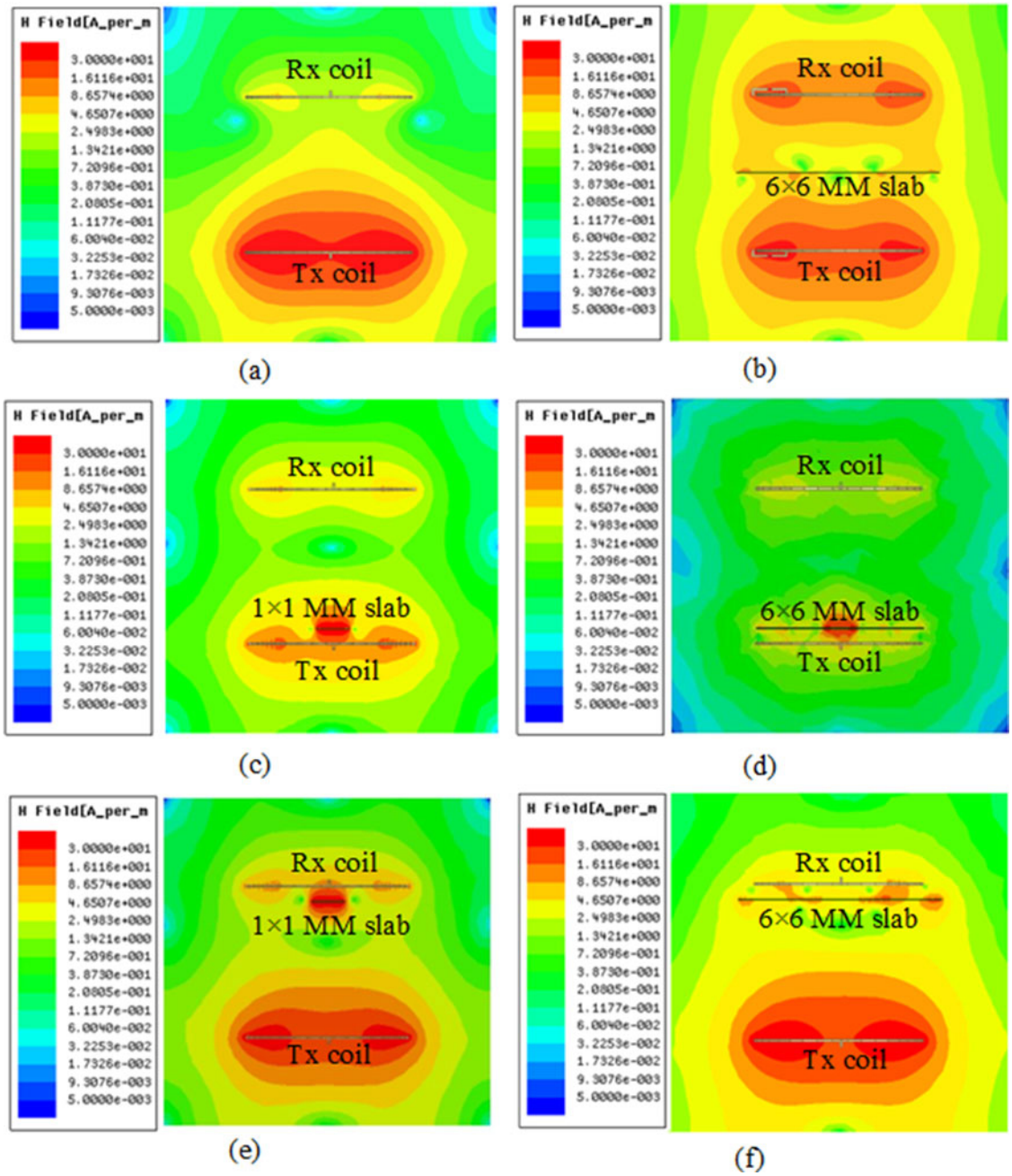


Figure 9. Comparison on magnetic field distribution of the MCR-WPT system: (a) without MM slab, (b) 6 × 6 MM slab in the middle, (c) 1 × 1 MM slab near the Tx coil, (d) 6 × 6 MM slab near the Tx coil, (e) 1 × 1 MM slab near the Rx coil, and (f) 6 × 6 MM slab near the Rx coil.

To observe the magnetic field distribution of the MCR-WPT system, an MCR-WPT system operating at 6.7 MHz is built in HFSS to perform simulation, as shown in Fig. 9(a). Moreover, the systems with 1 × 1 to 6 × 6 MM slabs placed in five different positions are also constructed. Figure 9(b)–(f) shows the results of different MM slabs at three positions in the system, respectively. Compared with the MCR-WPT system without the MM slab, the magnetic field intensity of the system with the MM slab is improved to varying degrees. When the MM slab is placed in the middle of the system, the improvement of the magnetic field distribution increases with the increase of arrays. When the MM slab is close to the Rx coil, the enhancement in the magnetic field distribution of the system is consistent with the trend in the middle position, but the improvement is slight. It is worth noting that only a 1 × 1 MM slab can improve the magnetic field density when it is close to the Tx coil, for the other arrays of MM slabs will significantly weaken the magnetic field density. It is demonstrated that the magnetic field is amplified by the negative permeability MM.

It can be seen from the simulation results that when the MM slab is in the center between the Tx coil and the Rx coil, the magnetic field is focused and enhanced after passing through the slab perpendicularly, thereby improving the PTE of the MCR-WPT system. Moreover, when the slab is placed near the Rx coil, since the magnetic field has already dissipated in the propagation,

https://doi.org/10.1017/S1759078723000582 Published online by Cambridge University Press

the effect of improving the transmission efficiency is small. However, when the MM slab is close to the Tx coil, the large size of the slab is responsible for the resonant frequency of the MCR-WPT system shifting, so the system is not resonant, and the PTE drops dramatically.

Experiment verification

The dual-coil MCR-WPT system is shown in Fig. 10, which consisted of the RF power supply, impedance matcher, Tx coil, Rx coil, oscilloscope, DC power source, supply voltage module, load resistor, and MM slabs. The RF power supply is responsible for inputting the alternating current of the operating frequency to the system, and the impedance matcher is used to obtain the maximum power output through the load impedance and the internal impedance of the excitation source to match each other. Due to the manufacturing errors of the coils, it is necessary to add tuning capacitors to ensure that the two coils resonate at 6.78 MHz to make the system reach maximum PTE.

For experiments, six periodical arrangement MM slabs are fabricated, as shown in Fig. 11. To study the effect of the MM slab on PTE, the MM slab is inserted in the system. The Rx coil is connected with a 60 Ω load. The power supply voltage module and the oscilloscope are used to measure the voltage across the load, and the PTE can be calculated by the output power and voltage values.

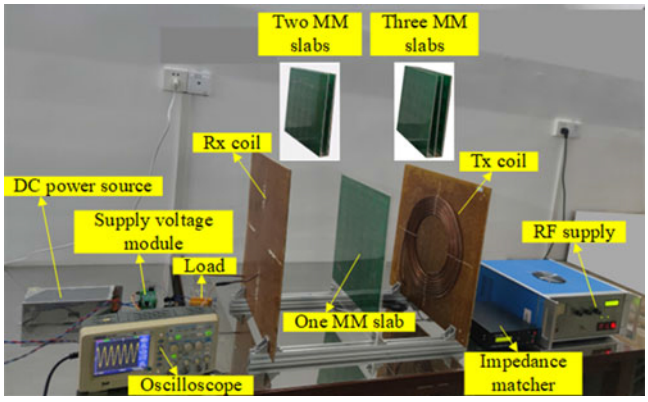


Figure 10. The experimental setup of the MCR-WPT system with MM slabs.

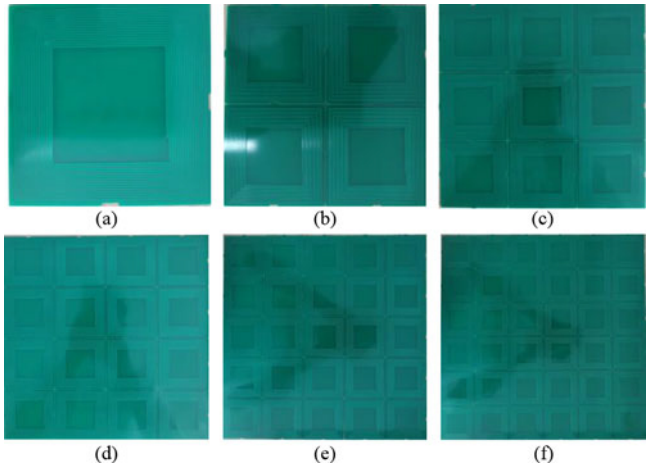


Figure 11. MM slabs of different periodic arrangements: (a) 1 × 1 array, (b) 2 × 2 arrays, (c) 3 × 3 arrays, (d) 4 × 4 arrays, (e) 5 × 5 arrays, and (f) 6 × 6 arrays.

Six kinds of MM slabs are placed in the middle of the system, the Tx coil, and the Rx coil, respectively. At the same time, the transmission distance of the system is changed and the change of the PTE of the system is measured. Fig. 12(a) shows the curve of the PTE change of the MM slabs when they are placed in the middle of the system, and it can be seen that the PTE increases with the increase of the period. It is worth noting that when the periodic arrangement changes from 1 × 1 to 3 × 3 arrays, the increase is small. When it is greater than 3 × 3 arrays, the PTE is significantly improved. The most improvement can be achieved when the slab is at 6 × 6 arrays, and the maximum efficiency improvement of 20.6% can be obtained. The PTE changes when the MM slab is placed near the Tx coil as shown in Fig. 12(b), and the efficiency can be improved by 9.2% at most under the condition when the array is 1 × 1. Compared with the middle position, the MM slab with a 1 × 1 array is more suitable to be placed near the Tx coil. However, the PTE will drop with the increase of the array. Figure 12(c) shows the

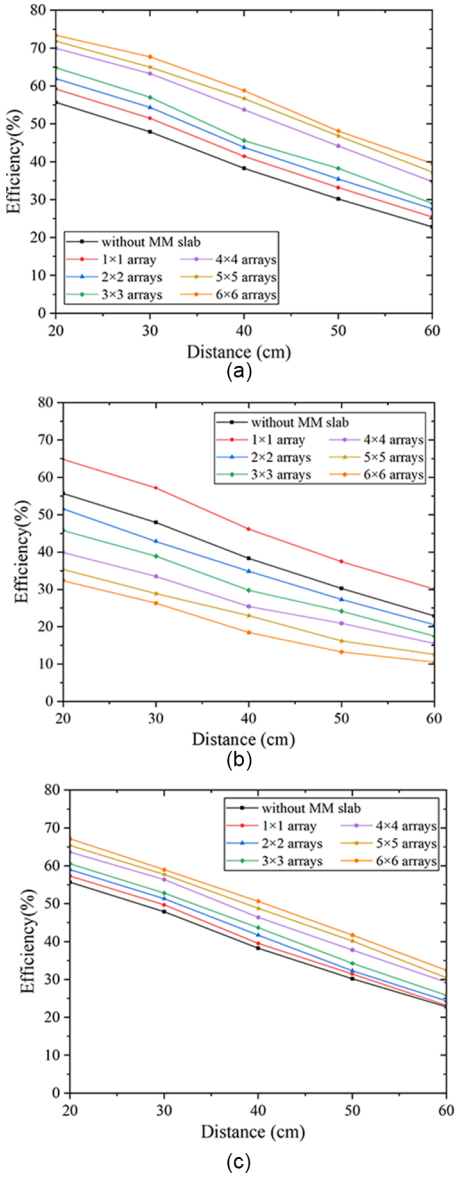


Figure 12. PTEs of MCR-WPT system with one MM slab: (a) in the middle, (b) near the Tx coil, and (c) near the Rx coil.

https://doi.org/10.1017/S1759078723000582 Published online by Cambridge University Press

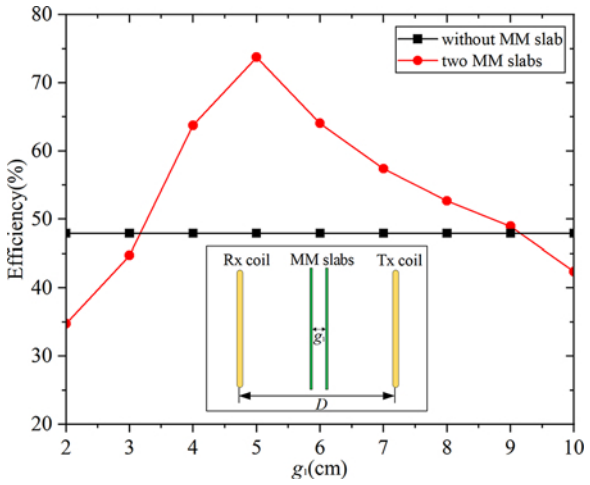


Figure 13. The relationship between the spacing of two MM slabs and PTEs.

curves of PTE changes when the MM slab is placed near the Rx coil. It can be seen that the influence of placing MM slabs with different periods near the Rx coil on the PTE is basically the same as that of placing them in the middle of the system, but the improvement is poor, even if the MM slab with 6 × 6 arrays can only be improved by 12.7% at most.

It can be concluded from the above results that when the MM slab is placed in the middle of the MCR-WPT system, the six kinds of arrays can all improve the PTE, and the maximum improvement is obtained by using a slab with 6 × 6 arrays. When the MM slab is closed to the Tx coil, only a 1 × 1 array can achieve the improvement for the system, but the improvement is small. Note that if the array exceeds 1 × 1, the PTE will drop. The reason for this phenomenon may be that the frequency splitting caused by the strong coupling between the MM slab and the MCR-WPT system in the near field leads to a significant drop in efficiency [22, 23]. When the MM slab is placed near the Rx coil, the trend is basically the same as when it is placed in the middle of the system, but the improvement effect is small. The experimental results indicate that MMs can achieve enhanced magnetic coupling and improve the PTE of the MCR-WPT system.

In order to further improve the PTE for MCR-WPT system, two MM slabs are used in the system. When two MM slabs are employed, it is necessary to investigate the influence of the spacing g_1 between two MM slabs on the PTE because g_1 is an important parameter. First, the distance between the Tx coil and the Rx coil is fixed at 30 cm and change the spacing of two slabs with 6 × 6 arrays. The relationship between PTE and g_1 is measured, and the result is shown in Fig. 13. It can be seen from figure that the curve of the PTE of the system changes with the increase of g. The highest PTE is 77.2% when $g_1 = 5$ cm. Compared with the system without MM slab, the PTE of the system with two slabs is improved by 29.3%.

Based on previous experiments, when two MM slabs are placed in three positions, respectively, their arrays are consistent with one slab. When two MM slabs are placed in the middle of the system, 6 × 6 arrays can obtain the optimal improvement. The experimental result is shown in Fig. 14(a); two MM slabs reach a maximum PTE improvement of 29.3% when the distance is 30 cm, which is 8.6% higher than one MM slab. Because the MM slab is placed near the Tx coil, only 1 × 1 array can improve the PTE, so two MM slabs with a 1 × 1 array are also inserted at the same position. The experimental result is shown in Fig. 14(b), and the PTE is obtained 13.1%

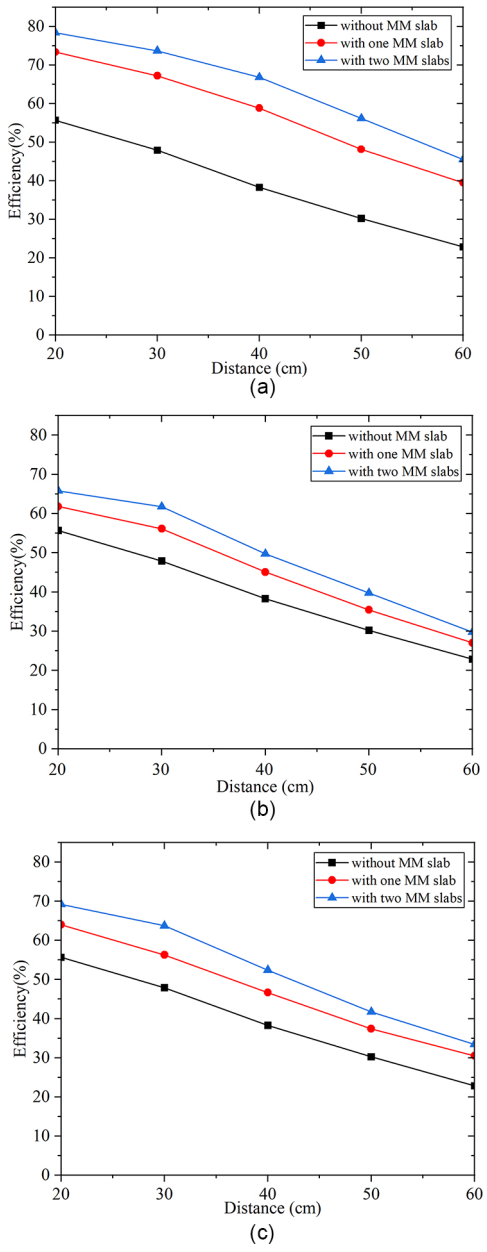


Figure 14. PTEs of MCR-WPT system with two MM slabs: (a) in the middle, (b) near the Tx coil, and (c) near the Rx coil.

at 30 cm, which is 3.9% higher than that of one MM slab. Fig. 14(c) shows the PTE change curve when two MM slabs with 6 × 6 arrays are placed close to the Rx coil, and the PTE is improved by 16.8%, which is 4.1% higher than that of one MM slab. Therefore, the magnetic field enhancement of two MM slabs is better than that of one slab, which can obtain a larger improvement for the PTE.

In addition, PTE of MCR-WPT with three MM slabs is also studied. Considering that the spacing g_2 between three MM slabs may be different from that of two slabs, it is also necessary to analyze the relationship between the PTE and spacing of three slabs. Similar to the previous measurement process, the transmission distance is also fixed at 30 cm, and three MM slabs are placed in the middle of the system. Change the spacing between slabs and measure the change in PTE to determine the optimal g_2. The results are shown in Fig. 15, and it can be seen that the PTE also rises with

https://doi.org/10.1017/S1759078723000582 Published online by Cambridge University Press

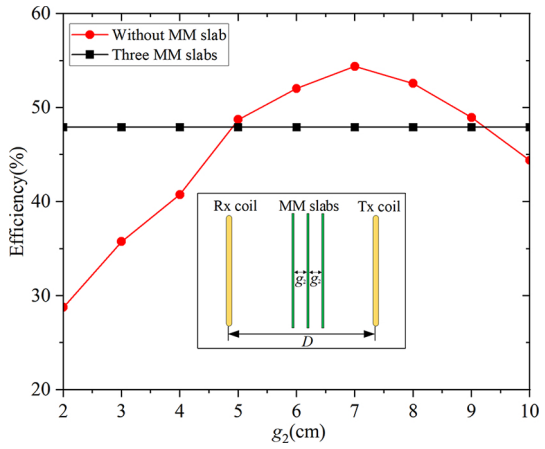


Figure 15. The relationship between the spacing of three MM slabs and PTEs.

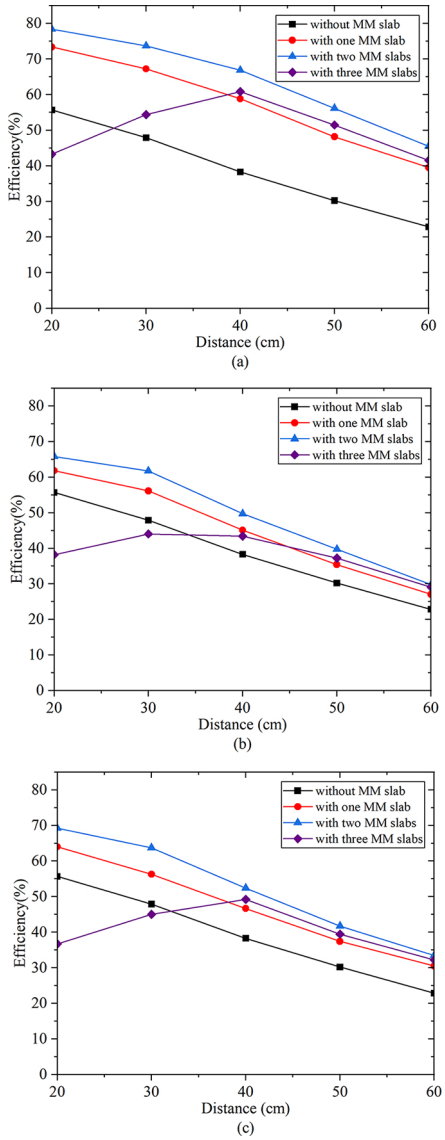


Figure 16. PTEs of MCR-WPT system with three MM slabs: (a) in the middle, (b) near the Tx coil, and (c) near the Rx coil.

Table 3. Comparison on highest PTE improvement under three cases.

	In the middle	Near the Tx coil	Near the Rx coil
One MM slab	20.6%	9.2%	12.7%
Two MM slabs	29.3%	13.1%	16.8%
Three MM slabs	22.6%	7.1%	10.9%

the increase of g_2 and then reaches the peak at 7 cm, and it finally decreases gradually.

In conclusion, the optimal g_2 of three MM slabs is 7 cm. Furthermore, PTEs of the system with three MM slabs are measured. Figure 16(a) shows the PTE of three MM slabs placed in the middle of the system, when the distance is less than 30 cm, and the PTE will be suppressed. When the distance is 30 cm, three slabs are positive for the system, but the improvement is weak. Once the distance is greater than 40 cm, the improvement is slightly higher than one MM slab, and the optimal improvement is 22.6%. The PTEs of the system with three MM slabs close to the Tx coil is shown in Fig. 16(b), and it can be seen that only when the distance exceeds 40 cm, three MM slabs can improve transmission performance and achieve a maximum improvement of 7.1% at 50 cm. Fig. 16(c) shows that when placing three MM slabs near the Rx coil, the trend is same as in the middle position, achieving a maximum improvement of 10.9% at a distance of 40 cm.

According to the above experimental results, it can be concluded that the MM slab can focus magnetic field to improve performance of MCR-WPT systems. A larger PTE improvement can be obtained by inserting two MM slabs, but the improvement of three MM slabs is poor. PTEs of the proposed MCR-WPT system with MM slabs under three conditions are compared specifically in Table 3.

Conclusion

In this paper, the principle of MCR-WPT with MMs is theoretically analyzed, indicating that MMs have great potential for improving efficiency. Then, to improve the PTE of MCR-WPT systems, a 6.78 MHz MCR-WPT system is established in HFSS software, and the MM unit is proposed for the system. It is shown that MMs can enhance the magnetic field between the Tx and Rx coils through many simulations. In order to verify the simulation results, the experimental setup of the MCR-WPT system and MM slabs are fabricated, and PTEs of the system are measured under different conditions. The experimental results demonstrated that when one MM slab is placed in the middle, near the Tx coil and the Rx coil, the highest PTE is obtained by adopting 6 × 6, 1 × 1, and 6 × 6 arrays, respectively. When a 6 × 6 MM slab is placed in the middle of the system, the PTE raises by 20.6%. Based on this, we also investigate PTEs of the system with multilayer MM slabs. The system with two MM slabs improves PTE by 29.3%, and the system with three MM slabs improves by 22.6%. Therefore, it can be concluded that the PTE improvement of two MM slabs is the best and that of one MM slab is the second but better than three MM slabs.

Acknowledgement. This work is supported in part by the National Natural Science Foundation of China under grant 61741126 and in part by the Guangxi Natural Science Foundation under grant 2022GXNSFAA035533.

https://doi.org/10.1017/S1759078723000582 Published online by Cambridge University Press

Competing interests. All authors declare that they have no known competing financial interests or relationships that could have appeared to influence the work reported in this paper.

References

1. **A Kurs, A Karalis, R Moffatt, JD Joannopoulos, P Fisher and M Soljačić** (2007) Wireless power transfer via strongly coupled magnetic resonances. *Science* **317**, 83–86.
2. **AK RamRakhyani, S Mirabbasi and M Chiao** (2011) Design and optimization of resonance-based efficient wireless power delivery systems for biomedical implants. *IEEE Transactions on Biomedical Circuits and Systems* **5**, 48–63.
3. **Q Li and YC Liang** (2015) An inductive power transfer system with a high-Q resonant tank for mobile device charging. *IEEE Transactions on Power Electronics* **30**, 6203–6212.
4. **CC Mi, G Buja, SY Choi and CT Rim** (2016) Modern advances in wireless power transfer systems for roadway powered electric vehicles. *Science* **63**, 6533–6545.
5. **J Kim, H-C Son, KH Kim and Y-J Park** (2011) Efficiency analysis of magnetic resonance wireless power transfer with intermediate resonant coil. *IEEE Antennas and Wireless Propagation Letters* **10**, 389–392.
6. **Q Deng, J Liu, D Czarkowski, MK Kazimierczuk, M Bojarski, H Zhou, W Hu** (2016) Frequency-dependent resistance of Litz-wire square solenoid coils and quality factor optimization for wireless power transfer. *IEEE Transactions on Industrial Electronics* **317**, 2825–2837.
7. **X Fan, F Tang, B Su and X Zhang** (2022) Design of spiral resonator based on fractal metamaterials and its improvement for MCR-WPT performance. *IEEE Transactions on Magnetics* **58**, 1–9.
8. **K Sun, R Fan, X Zhang, Z Zhang, Z Shi, N Wang, P Xie, Z Wang, G Fan, H Liu, C Liu, T Li, C Yan, Z Guo** (2018) An overview of metamaterials and their achievements in wireless power transfer. *Journal of Materials Chemistry C* **6**, 2925–2943.
9. **X Zhang and Z Liu** (2008) Superlenses to overcome the diffraction limit. *Nature Materials* **7**, 435–441.
10. **J Valentine, J Li, T Zentgraf, G Bartal and X Zhang** (2009) An optical cloak made of dielectrics. *Nature Materials* **8**, 568–571.
11. **MJ Freire, L Jelinek, R Marques and M Lapine** (2010) On the applications of $\mu_r = -1$ metamaterial lenses for magnetic resonance imaging. *Journal of Magnetic Resonance* **203**, 81–90.
12. **J Choi and CH Seo** (2010) High-efficiency wireless energy transmission using magnetic resonance based on negative refractive index metamaterial. *Progress in Electromagnetics Research* **106**, 33–47.
13. **Y Urzhumov and DR Smith** (2011) Metamaterial-enhanced coupling between magnetic dipoles for efficient wireless power transfer. *Physical Review B* **83**, 205114.
14. **W Li, P Wang, C Yao, Y Zhang, and H Tang** (2016) Experimental investigation of 1D, 2D, and 3D metamaterials for efficiency enhancement in a 6.78 MHz wireless power transfer system. *IEEE Wireless Power Transfer Conference (WPTC)*. Aveiro: IEEE.
15. **VG Veselago** (1968) The electrodynamics of substances with simultaneously negative values of permittivity and permeability. *Soviet Physics Uspekhi* **10**, 509–514.
16. **RA Shelby, DR Smith and S Schultz** (2001) Experimental verification of a negative index of refraction. *Science* **292**, 77–79.
17. **JB Pendry** (2000) Negative refraction makes a perfect lens. *Physical Review Letters* **85**, 3966–3969.
18. **A Ishimaru, S-W Lee, Y Kuga and V Jandhyala** (2003) Generalized constitutive relations for metamaterials based on the quasi-static Lorentz theory. *IEEE Transactions on Antennas and Propagation* **51**, 2550–2557.
19. **L Li, H Liu, H Zhang and W Xue** (2018) Efficient wireless power transfer system integrating with metasurface for biological applications. *IEEE Transactions on Industrial Electronics* **65**, 3230–3239.
20. **DR Smith, DC Vier, T Koschny and CM Soukoulis** (2005) Electromagnetic parameter retrieval from inhomogeneous metamaterials. *Physical Review E* **71**, 36617–36628.
21. **Z Szabó, G-H Park, R Hedge and E-P Li** (2010) A unique extraction of metamaterial parameters based on Kramers–Kronig relationship. *IEEE Transactions on Microwave Theory and Techniques* **58**, 2646–2653.
22. **Y Zhang, Z Zhao, and K Chen** (2013) Frequency splitting analysis of magnetically-coupled resonant wireless power transfer. *IEEE Energy Conversion Congress and Exposition (ECCE)*, Denver (IEEE).
23. **C Zhao, S Zhu, H Zhu, Z Huang, X Luo** (2018) Accurate design of deep sub-wavelength metamaterials for wireless power transfer enhancement. *Progress in Electromagnetics Research* **83**, 195–203.



Xingming Fan received the Ph.D. degree in Mechatronic Engineering from Dalian University of Technology, Dalian, China, in 2007. He is currently a professor with the Department of Electrical Engineering and Automation, Guilin University of Electronic Technology. His major research interest includes intelligent apparatus, electrical measurement, and high-voltage technology.



Haonan Zhang received the B.S. degree in College of Mechanical and Control Engineering from Guilin University of Technology, Guilin, China, in 2016. He is currently pursuing the M.S. degree in Electrical Engineering and Automation from Guilin University of Electronic Technology, Guilin, China. His major research interest includes intelligent apparatus.



Xin Zhang is currently an Expert Experimenter with the Department of Mechanical Engineering, Guilin University of Electronic Technology. Her major research interest includes intelligent apparatus.

https://doi.org/10.1017/S1759078723000582 Published online by Cambridge University Press